fibers

MDPI

Article

Effect of Nested Elements on Avoided Crossing between the Higher-Order Core Modes and the Air-Capillary Modes in Hollow-Core Antiresonant Optical Fibers

Laurent Provino

PERFOS, Research Technology Organization of Photonics Bretagne, 4 rue Louis de Broglie, 22300 Lannion, France; lprovino@photonics-bretagne.com

Received: 14 May 2018; Accepted: 13 June 2018; Published: 18 June 2018

Abstract: Optimal suppression of higher-order modes (HOMs) in hollow-core antiresonant fibers comprising a single ring of thin-walled capillaries was previously studied, and can be achieved when the condition on the capillary-to-core diameter ratio is satisfied ($d/D \approx 0.68$). Here we report on the conditions for maximizing the leakage losses of HOMs in hollow-core nested antiresonant node-less fibers, while preserving low confinement loss for the fundamental mode. Using an analytical model based on coupled capillary waveguides, as well as full-vector finite element modeling, we show that optimal d/D value leading to high leakage losses of HOMs, is strongly correlated to the size of nested capillaries. We also show that extremely high value of degree of HOM suppression (∼1200) at the resonant coupling is almost unchanged on a wide range of nested capillary diameter d_{Nested} values. These results therefore suggest the possibility of designing antiresonant fibers with nested elements, which show optimal guiding performances in terms of the HOM loss compared to that of the fundamental mode, for clearly defined paired values of the ratios d_{Nested}/d and d/D. These can also tend towards a single-mode behavior only when the dimensionless parameter d_{Nested}/d is less than 0.30, with identical wall thicknesses for all of the capillaries.

Keywords: hollow-core antiresonant fiber; numerical modeling; modal fiber properties

1. Introduction

A new form of silica hollow-core fiber consisting of a single ring of touching or non-touching antiresonant elements (ARE) surrounding a central hollow-core has emerged in recent years. This antiresonant fiber (ARF) has been investigated as a result of the discovery of the importance of core wall shape in the attenuation reduction in Kagome-structured hollow-core fiber in 2010 [1]. Accordingly, it was possible to reduce the Kagome cladding to just one single glass layer of ARE without significantly increasing fiber attenuation [2]. Thereafter, different hollow core fibers comprising a single ring of touching capillaries in the cladding void have been proposed and studied. It was proven that ARFs, with an inverted optical core boundary, possess large transmission bandwidth and low attenuations in the mid-infrared spectral region due to both low leakage losses and weak coupling of air-core modes with the cladding structure [3–5]. This type of design was extended to shorter wavelength transmission in the near-infrared and visible spectrum [6,7]. A modified form of the basic design with contactless capillaries has also been proposed and fabricated in order to remove the additional optical resonances in the transmission bands related to nodes between cladding elements [8]. In this way, the loss level can be further decreased in the mid-infrared wavelength range [8,9]. Recently, greatly reduced transmission loss at 750 nm in similar fiber was reported by Debord et al. [10]. By adding one or more nested capillaries within the node-less cladding structure,

numerical simulations predicted leakage losses reduction by roughly two orders of magnitude in the middle and near infrared spectral regions [11,12]. Up to now, the fabrication of at least two fibers with nested antiresonant node-less elements (NANFs) has been reported for low loss operation. The fibers have been manufactured both with different [13] and closely identical [14] wall thicknesses between the inner and outer cladding capillaries. The wall thickness of the large capillaries was greater than a micrometer. According to performances of theses fabricated fibers, the positive effect of the nested capillaries on the loss is limited by their small hole diameter and the distinction between the wall thicknesses of the large and small capillaries. However, a minimum optical loss of 74 dB/km at 1.8 μm was obtained in a NANF with a 25 μm core diameter and a 2.3 μm average wall thickness of all the capillaries [14]. The leakage loss in the ARFs, as in the NANFs, is inversely proportional to the fourth power of core diameter [15], so lower losses are much easier to achieve at larger core diameters. For large core diameters (>25 μm), the ARFs and NANFs are however multimoded [11] and therefore not ideal for applications where a high modal purity is desirable, for example in high-power pulse delivery or in gas cells. To suppress HOMs while preserving low confinement loss for the fundamental core mode, a technique has already been proposed for different designs of ARFs with touching and non-touching capillaries [16–18]. It exploits resonant coupling between the higher-order core modes and the air-capillary modes. The approach is analogous to using defect modes in HC-PCFs [19,20]; however, there is no need to create defects in this case, since the capillaries that create cladding structure can also provide the resonant coupling. Specifically Uebel et al. [17] showed the importance of the dimensionless parameter d/D, with the inner capillary diameter d and the inner core diameter D, in order to achieve optimal suppression of HOMs over all wavelength bands where the ARF guides with low loss. For 6- and 7-capillary designs [17,18], an avoided crossing between TM_{01}, TE_{01}, and HE_{21} core modes and fundamental air-capillary mode is observed at $d/D \approx 0.68$ which leads to high leakage losses of those HOMs and hence, provides robust single-mode guidance at all wavelengths within the main transmission window, independent of the absolute core size of the structure. This condition on the capillary-to-core diameter can also be verified for any ARF structures composed of a smaller number of capillaries. However, a number of capillaries less than six would lead to a pronounced gap between capillaries that can affect the fundamental mode loss.

The purpose of this work is to study the impact that the nested elements can have on the avoided crossing between the higher-order core modes and the air-capillary modes, in order to verify that the condition of HOM suppression established for the ARFs could be applied or not to NANFs. We show computationally that it is also possible to suppress the HOMs in NANFs; however, the optimal d/D value, for which the leakage losses of HOMs are maximum, is strongly dependent on the geometric dimension of nested capillaries. The numerical results are also interpreted and verified by extending an already proposed analytical model based on coupled capillaries.

2. Design and Numerical Analysis

In order to analyze the influence of nested elements on the modal properties of ARFs, we propose in this work to maintain the six node-less capillary lattice structure described in [17] and add nested capillaries of inner diameter d_{Nested} with the same wall thickness t_{Nested} as the outer ones and attached to the cladding at the same azimuthal position, as shown in the left panel of Figure 1. Considering the fact that both the transmission band positions [11,12,16,17] and the leakage losses [13] are dependent on the wall thickness of the capillaries, the choice of setting $t_{Nested} = t$ allows for avoiding additional effects on the present study.

All numerical simulations reported here are based on a commercial full-vector finite-element based modal solver (Comsol Multiphysics). A circular Perfectly Matched Layer (PML) surrounding the simulated area is used to calculate the mode leakage losses. Only a quarter of the geometry is used in modeling fibers because of the symmetry of the modes [21]. As in [17], we adopted a core diameter $D = 30$ μm, a silica wall thickness $t = 0.30$ μm and a wavelength $\lambda = 1.50$ μm, in such a way that the ratios t/D and D/λ are equal to 0.01 and 20, respectively. The glass refractive index was set a constant

value of 1.45 and the hollow regions were taken to be vacuum. The material loss is neglected since the material absorption is quite low at this wavelength [22].

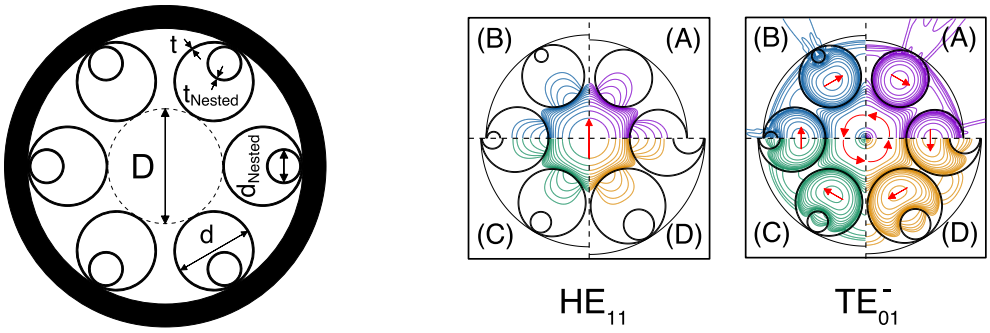

Figure 1. Left: Sketch of the Nested Antiresonant Node-less Fiber (NANF) cross-section, with its key parameters. Glass is marked in black and the hollow regions in white. Right: 3-dB contour plots of the HE_{11} fundamental modes and hybrid TE_{01}^{-} modes at the avoided crossing point, for different values of d_{Nested}/d equal to 0.00 (A), 0.20 (B), 0.30 (C) and 0.40 (D) respectively. The color code used is identical to that in Figure 2. The contour plots represent the normalized electric field intensity and the red arrows indicate the polarization direction of the transverse electric field.

In order to model NANF accurately, great care was taken to optimize both mesh and PML parameters. Typically, a maximum element size of $\lambda/4$ was used in the air regions while a rather dense mesh with a maximum element size of $\lambda/6$ in the thin glass regions was found to be essential to obtain reliable results. To ensure convergence of the numerical results, we first checked our model by reproducing the results of the [17] ($d_{Nested}/d = 0$), and afterward the modal properties for the first guided modes were simulated for d_{Nested}/d ratio respectively equal to 0.20, 0.30 and 0.40.

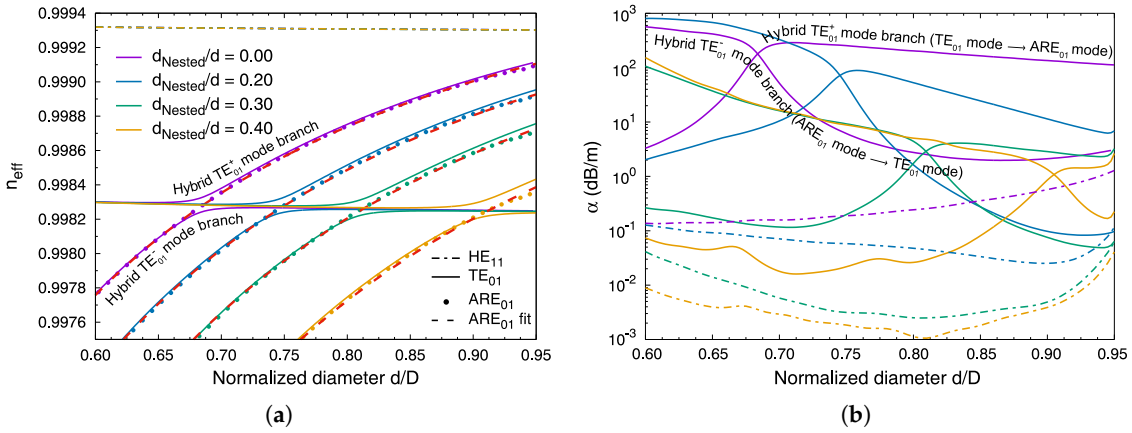

(**a**) (**b**)

Figure 2. Numerically computed modal properties d/D dependence for different values of d_{Nested}/d with $t/D = 0.01$ and $D/\lambda = 20$. (**a**) Effective indices of the fundamental HE_{11} core mode (dot dashed curves), hybrid TE_{01}^{+} and TE_{01}^{-} modes (solid curves) and ARE_{01} air-capillary mode (dotted curves). The red dashed curve for each d_{Nested}/d value represents the effective index of the ARE_{01} mode of an isolated capillary, using the analytic model. (**b**) Corresponding mode confinement loss.

Figure 2a shows the effective index for the fundamental HE_{11} core mode, the TE_{01} core mode, and the ARE_{01} air-capillary mode as a function of the radio d/D. The TE_{01} mode is the higher-order core mode that has the lowest loss, and also the lowest effective index difference with the fundamental HE_{11} mode. Note that, according to the polarization profile of the guided modes, the core modes are indicated using the designation of vector modes HE_{nm}, EH_{nm}, TE_{0m} and TM_{0m} with n and m integers and the air-capillary mode of the node-less cladding structure is labeled ARE_{lm} with l and m integers,

based on the notation of the linearly polarized modes. Figure 2b shows the corresponding confinement loss of the core modes.

For $d_{Nested}/d = 0$, we find again in Figure 2a the discontinuity of the TE_{01} core mode effective index for $0.62 < d/D < 0.75$ as in [17], typical of an avoided crossing between the core localized mode (herein the TE_{01} mode) and a cladding leaky mode (herein the ARE_{01} mode) [23]. In this region of d/D values, the TE_{01} core mode splits into two hybrid modes labelled TE_{01}^{+} and TE_{01}^{-}, which evolve asymptotically in toward uncoupled ARE_{01} and TE_{01} modes. Indeed for largest values of effective index, the TE_{01} core mode gradually changes its nature to become an ARE_{01} air-capillary mode and conversely for smaller values of effective index, the ARE_{01} air-capillary mode progressively converges toward a TE_{01} core mode. For non-zero values of the ratio d_{Nested}/d, the evolution of the TE_{01} core mode effective index as a function of d/D is similar. However, we observe an increasing shift in the position of the discontinuity in relation to d/D when the ratio d_{Nested}/d rises. As with the d/D parameter, these numerical results show the importance of the nested capillaries's diameter on avoided crossing between the TE_{01} core mode and the ARE_{01} air-capillary mode, and the scalability of this phenomenon through the dimensionless parameter d_{Nested}/d. On the other hand, the effective index of the HE_{11} core mode remains independent of d/D, regardless of the d_{Nested}/d value.

To quantify the avoided crossing properties, we introduce the quantity $\mathfrak{D} = \partial^2 \Re e(n_{eff})/\partial(d/D)^2$. By analogy with chromatic dispersion, we can associate this quantity with the effective index dispersion of a mode in relation to d/D. In Figure 3a, we plotted the obtained curves for the four values of the parameter d_{Nested}/d. For each transition region, we observe that the effective index dispersion curve exhibits a concave profile and large positive coefficient around a specific $(d/D)_{max}$ value corresponding at the phase-matching to resonance point $(n_{eff}^{TE_{01}} = n_{eff}^{ARE_{01}})$. These values are summarized in Table 1. The numerical result presented for $d_{Nested}/d = 0$ is in good agreement with that of the [17], and thus ensures the validity of the optimal values for the ratio $d_{Nested}/d > 0$ for which an avoided crossing between the TE_{01} core mode and the ARE_{01} air-capillary mode exists. Similarly to what was already described in [24], the strength of the interaction between the core mode and the air-capillary mode or, in other words, the degree of overlap between the fields of the two modes is proportional to the magnitude of the d/D range over which the transformation takes place, and is conversely in proportion to the peak value that is smoothed. As a result, we can deduce that an increase of the nested capillary's diameter induces a stronger coupling between these modes because the full width at half maximum Δ_{FWHM} of the curves increases slightly with the d_{Nested}/d parameter and the peak value at $(d/D)_{max}$ decreases. This increased interaction is related to the nested capillaries which increasingly squeeze the air-capillary modes towards the fiber core when their sizes increase (see Figure 1 at the right).

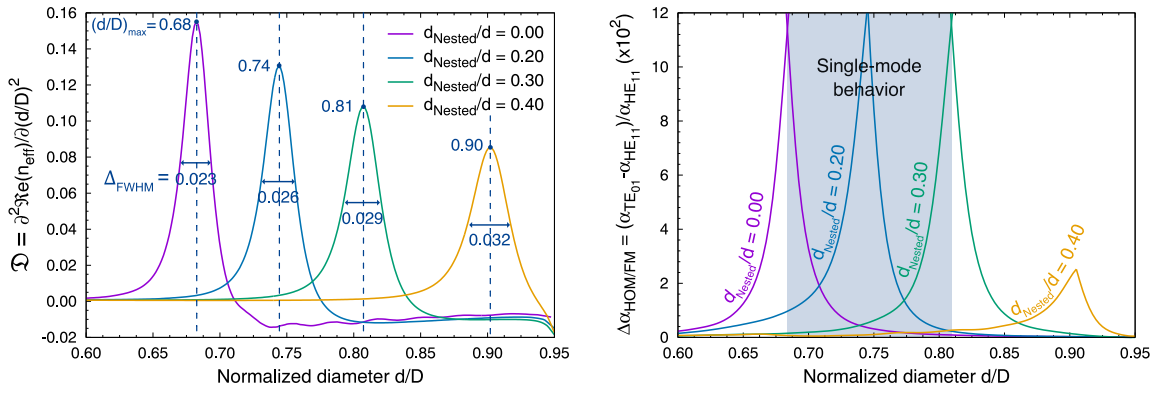

Figure 3. (**a**) Effective index dispersion of the TE_{01}^{+} hybrid mode as a function of normalized diameter d/D, for four different values of parameter d_{Nested}/d; (**b**) Numerically calculated degree of HOM suppression, plotted against d/D using the simulated confinement losses above. The gray-shaded area shows the region where NANFs tend towards a single-mode behavior.

Table 1. Summary of main results and parameters.

d_{Nested}/d	$(d/D)_{max}$	Δ_{FWHM}	$(d/D)_{th}$	f_{co}	f_{cl}
0.00	0.68	0.023	0.68	1.07	0.98
0.20	0.74	0.026	0.75	1.07	0.90
0.30	0.81	0.029	0.81	1.07	0.83
0.40	0.90	0.032	0.91	1.07	0.73

In terms of confinement loss, we observe in each case that the loss of the two hybrid modes strongly increases up to the avoided crossing point and then slowly varies beyond the $(d/D)_{max}$ value. Conversely, the HE_{11} core mode has a weakly fluctuating low loss over the value range of d/D, independently of the set value of the d_{Nested}/d ratio. We thus find the same performances in the evolution of the losses in respect to d/D as described in [17] for the HE_{11} and hybrid $TE_{01}^{+,-}$ modes, which makes it possible to consider finding NANF designs with a strong degree of HOM suppression compared to the fundamental mode, defined as [17]

$$\Delta\alpha_{\mathrm{HOM/FM}} = \frac{\alpha_{HOM} - \alpha_{FM}}{\alpha_{FM}} \tag{1}$$

where α_{FM} and α_{HOM} are the losses of the HE_{11} and hybrid $TE_{01}^{+,-}$ modes (in dB/m), respectively. This relation can give an indication of the single-modeness of the given fiber. However, the addition of nested capillaries decreases the overall losses for all guided modes between one to two orders of magnitude depending on the size of the nested AREs. For NANFs consisting of six nested elements with a ratio $d_{Nested}/d \geq 0.30$, the suppression of higher-order core modes while satisfying the condition on the parameter d/D can become problematic. This is due to the fact that the nested capillaries and the narrow inter-capillary distance effectively shield the electric field leaking into the silica outer cladding (see Figure 1 on the right hand side). A sufficiently large loss level cannot hence be reached for the higher-order TE_{01} mode. In Figure 3b the calculated degree of HOM suppression strongly increases at the anti-crossing position, peaking at the values around 1200 for the first three values of d_{Nested}/d. When $d_{Nested}/d = 0.40$, this value drops at ~250. The degree of HOM suppression for $d_{Nested}/d = 0.30$ is similar to that without nested capillaries, whereas the loss is almost two orders of magnitude smaller for the two core modes. Whatever the value of d_{Nested}/d, the single-mode or multimode behavior of NANF can only be defined with respect to the length of fiber needed to develop new applications, such as light-sources/lasers emitting in the deep-UV/UV or the mid-infrared. If only a few meters of fiber are sufficient so that the losses of the HE_{11} and TE_{01} core modes are practically negligible over this length (as for $d_{Nested}/d = 0.30$), in spite of the fact the TE_{01} mode presents 1000 times higher loss, it will not actually be effectively suppressed. Thus, in order to verify the single-mode behavior of NANFs over a specified wavelength interval, estimating the degree of HOM suppression is a necessary but not sufficient criteria and the lowest loss estimation of higher-order core modes is most important.

3. Analytical Model

To understand and predict the avoided crossings in ARFs with touching or non-touching capillaries, an analytical model in which the core and the cladding of AREs are treated as two coupled capillaries has been proposed in the [16,17]. We propose here to apply this analytical model to NANFs depicted in Figure 1. Generally, the effective index of guided modes in the inner region of capillary with infinite wall thickness can be estimated by the Marcatili-Schmeltzer formula [25], rewritten as

$$n_{eff}^{co,\,cl} = n_L - \frac{1}{2}\left(\frac{u_{pm}^{co,\,cl}}{\pi\sqrt{n_L}}\right)^2\left(\frac{\lambda}{d_{eff}^{co,\,cl}}\right)^2 \tag{2}$$

where the exponents *co* and *cl* indicate the capillary linked to the core and the cladding, respectively; n_L the refractive index of inner medium made of air ($n_L = n_{air} = 1$) ; the coefficient $u_{pm}^{co,\,cl}$ is the m-th

zero of the Bessel function $J_p(u_{pm}) = 0$, with $p = n$ for vector modes and $p = l + 1$ for linearly polarized modes. The effective diameter $d_{eff}^{co} = f_{co} \times D$ or $d_{eff}^{cl} = f_{cl} \times d$ is the inner diameter of the capillary. The coefficients f_{co} and f_{cl} are used to adjust the value of diameters d and D in order to match the analytical values from Equation (2) to the numerical results of finite-element simulations. In Figure 2a, are plotted the fitted values for each ARE_{01} air-capillary mode (red dashed curves) calculated using Equation (2) with the fitting coefficients f_{cl} reported in Table 1. Analytical and numerical computed values are in excellent agreement. The dependence of the coefficient f_{cl} with respect to the dimensionless parameter d_{Nested}/d can be related to the space filling rate of the nested capillaries inside the outer ones. Indeed we observe in Figure 2a that the more the nested capillary diameter increases, the more the effective index of theARE_{01} air-capillary mode decreases with both parameters D and d held constant. According to (2), the combination of two nested capillaries can then be defined by a single capillary with an effective diameter of smaller size. For the HE_{11} core mode, the effective index value showing a very low variation at constant core diameter ($D = 30$ µm), the application of Equation (2) allows by taking the average of the effective indices for each value of d_{Nested}/d to find a constant value of the fitting coefficient f_{co} equal to 1.07. We verified that this increase in core diameter by 7% can be applied to the first four higher-order core modes and found that the effective indices of the $HE_{21}^{even,\,odd}$, TM_{01} and TE_{01} core modes in NANFs match the effective indices of the modes in the corresponding capillary with a precision of order to 10^{-5}. At the avoided crossing point of the coupled modes, the equivalence of effective indices between the TE_{01} core mode and ARE_{01} air-capillary mode by using Equation (2) allows to derive a simple expression for the d/D parameter

$$n_{eff}^{co} = n_{eff}^{cl} \quad \Rightarrow \quad \left(\frac{d}{D}\right)_{th} = \frac{u_{11}^{cl}}{u_{01}^{co}} \cdot \frac{f_{co}}{f_{cl}(d_{Nested}/d)} \tag{3}$$

in which the value of coefficient $f_{cl}(d_{Nested}/d)$ depends on the value of the ratio d_{Nested}/d. The calculated theoretical values of $(d/D)_{th}$ from Equation (3) are summarized in Table 1 and are in good agreement with the $(d/D)_{max}$ values obtained from finite-element modeling. Thus, the analytical model based on coupled capillaries can be extended to NANFs and allows a simple prediction of the avoided crossing between the higher-order core modes and the air-capillary modes.

4. Conclusions

We investigated numerically and analytically the effect of nested thin-walled capillaries on the modal properties of a hollow-core fiber consisting of a single ring of six non-touching capillaries of the same wall thickness, mounted inside a thick-walled glass capillary. We observed a dependence with respect to the dimensionless parameter d_{Nested}/d on the $(d/D)_{max}$ value at which the resonant coupling between the higher-order core modes and an air-capillary mode, characterized by an avoided crossing and an extremely high degree of HOM suppression, is optimal. This leads to the possibility of designing a large range of NANFs with optimal transmission performances. However, we have noted that a high degree of mode suppression does not necessarily mean that the fibre is single-mode. The NANFs will perform effectively as a single-mode fiber, when the loss of the HOM are significantly higher (>30 dB/m) than that of the fundamental mode, for fiber lengths of a few meters. For values of $d_{Nested}/d < 0.30$, the NANFs can then tend towards a single-mode behavior, with performance in confinement loss superior to ARFs, for the fundamental mode. However, this type of NANFs seem much more difficult to fabricate than ARFs, compared to attempts made for at least three years. Indeed, for NANFs with a core diameter between 30 µm and 50 µm, the nested capillary diameters will not exceed 10 µm when $d_{Nested}/d < 0.30$, with the same wall-thickness as the outer capillaries of dimensions smaller than or of the order of micrometer. Therefore, there is a trade-off between transmission performance and technological difficulties related to fiber design.

Funding: This work is supported in part by the "Conseil Régional de Bretagne" and the "Fonds Européen de Développement Economique des Régions".

Acknowledgments: The author would like to thank Thierry Taunay for useful discussions throughout the work.

Conflicts of Interest: The authors declare no conflict of interest.

References

1. Wang, Y.Y.; Couny, F.; Roberts, P.J.; Benabid, F. Low loss broadband transmission in optimized core-shape Kagome hollow-core PCF. In Proceedings of the Lasers Electro-Optics, Quantum Electron, Laser Science Conference, San Jose, CA, USA, 16–21 May 2010; pp. 1–2.
2. Gérôme, F.; Jamier, R.; Auguste, J.L.; Humbert, G.; Blondy, J.M. Simplified hollow-core photonic crystal fiber. *Opt. Lett.* **2010**, *35*, 1157–1159. [CrossRef] [PubMed]
3. Pryamikov, A.D.; Biriukov, A.S.; Kosolapov, A.F.; Plotnichenko, V.G.; Semjonov, S.L.; Dianov, E.M. Demonstration of a waveguide regime for a silica hollow-core microstructured optical fiber with a negative curvature of the core boundary in the spectral region >3.5 µm. *Opt. Express* **2011**, *19*, 1441–1448. [CrossRef] [PubMed]
4. Yu, F.; Wadsworth, W.J.; Knight, J.C. Low loss silica hollow core fibers for 3–4 µm spectral region. *Opt. Express* **2012**, *20*, 11153–11158. [CrossRef] [PubMed]
5. Yu, F.; Knight, J.C. Spectral attenuation limits of silica hollow core negative curvature fiber. *Opt. Express* **2013**, *21*, 21466–21471. [CrossRef] [PubMed]
6. Jaworski, P.; Yu, F.; Maier, R.R.J.; Wadsworth, W.J.; Knight, J.C.; Shephard, J.D.; Hand, D.P. Picosecond and nanosecond pulse delivery through a hollow-core Negative Curvature Fiber for micro-machining applications. *Opt. Express* **2013**, *21*, 22742–22753. [CrossRef] [PubMed]
7. Jaworski, P.; Yu, F.; Carter, R.M.; Knight, J.C.; Shephard, J.D.; Hand, D.P. High energy green nanosecond and picosecond pulse delivery through a negative curvature fiber for precision micro-machining. *Opt. Express* **2015**, *23*, 8498–8506. [CrossRef] [PubMed]
8. Kolyadin, A.N.; Kosolapov, A.F.; Pryamikov, A.D.; Biriukov, A.S.; Plotnichenko, V.G.; Dianov, E.M. Light transmission in negative curvature hollow core fiber in extremely high material loss region. *Opt. Express* **2013**, *21*, 9514–9519. [CrossRef] [PubMed]
9. Belardi, W.; Knight, J.C. Hollow antiresonant fibers with low bending loss. *Opt. Express* **2014**, *22*, 10091–10096. [CrossRef] [PubMed]
10. Debord, B.; Amsanpally, A.; Chafer, M.; Baz, A.; Maurel, M.; Blondy, J.M.; Hugonnot, E.; Scol, F.; Vincetti, L.; Gérôme, F.; et al. Ultralow transmission loss in inhibited-coupling guiding hollow fibers. *Optica* **2017**, *4*, 209–217. [CrossRef]
11. Poletti, F. Nested antiresonant nodeless hollow core fiber. *Opt. Express* **2014**, *22*, 23807–23828. [CrossRef] [PubMed]
12. Habib, M.S.; Bang, O.; Bache, M. Low-loss hollow-core silica fibers with adjacent nested anti-resonant tubes. *Opt. Express* **2015**, *23*, 17394–17406. [CrossRef] [PubMed]
13. Belardi, W. Design and Properties of Hollow Antiresonant Fibers for the Visible and Near Infrared Spectral Range. *J. Lightwave Technol.* **2015**, *33*, 4497–4503. [CrossRef]
14. Kosolapov, A.F.; Alagashev, G.K.; Kolyadin, A.N. Hollow-core revolver fibre with a double-capillary reflective cladding. *Quantum Electron.* **2016**, *46*, 267–270. [CrossRef]
15. Vincetti, L. Empirical formulas for calculating loss in hollow core tube lattice fibers. *Opt. Express* **2016**, *24*, 10313–10325. [CrossRef] [PubMed]
16. Wei, C.; Kuis, R.A.; Chenard, F.; Menyuk, C.R.; Hu, J. Higher-order mode suppression in chalcogenide negative curvature fibers. *Opt. Express* **2015**, *23*, 15824–15833. [CrossRef] [PubMed]
17. Uebel, P.; Günendi, M.C.; Frosz, M.H.; Ahmed, G. Broadband robustly single-mode hollow-core PCF by resonant filtering of higher-order modes. *Opt. Lett.* **2016**, *41*, 1961–1964. [CrossRef] [PubMed]
18. Michieletto, M.; Lyngsø, J.K.; Jakobsen, C.; Lægsgaard, J.; Bang, O.; Alkeskjold, T.T. Hollow-core fibers for high power pulse delivery. *Opt. Express* **2016**, *24*, 7103–7120. [CrossRef] [PubMed]
19. Fini, J.M.; Nicholson, J.W.; Windeler, R.S.; Monberg, E.M.; Meng, L.; Mangan, B.; DeSantolo, A.; DiMarcello, F.V. Low-loss hollow-core fibers with improved single-modedness. *Opt. Express* **2013**, *21*, 6233–6242. [CrossRef] [PubMed]

20. Saitoh, K.; Florous, N.J.; Murao, T.; Koshiba, M. Design of photonic band gap fibers with suppressed higher-order modes: Towards the development of effectively single mode large hollow-core fiber platforms. *Opt. Express* **2006**, *14*, 7342–7352. [CrossRef] [PubMed]
21. McIsaac, P. Symmetry-Induced Modal Characteristics of Uniform Waveguides—I: Summary of Results. *IEEE Trans. Microw. Theory Tech.* **1975**, *23*, 421–429. [CrossRef]
22. Pilon, L.; Jonasz, M.; Kitamura, R. Optical constants of silica glass from extreme ultraviolet to far infrared at near room temperature. *Appl. Opt.* **2007**, *46*, 8118–8133.
23. Renversez, G.; Boyer, P.; Sagrini, A. Antiresonant reflecting optical waveguide microstructured fibers revisited: A new analysis based on leaky mode coupling. *Opt. Express* **2006**, *14*, 5682–5687. [CrossRef] [PubMed]
24. Engeness, T.D.; Ibanescu, M.; Johnson, S.G.; Weisberg, O.; Skorobogatiy, M.; Jacobs, S.; Fink, Y. Dispersion tailoring and compensation by modal interactions in OmniGuide fibers. *Opt. Express* **2003**, *11*, 1176–1196. [CrossRef]
25. Marcatili, E.A.J.; Schmeltzer, R.A. Hollow metallic and dielectric waveguides for long distance optical transmission and lasers. *Bell Syst. Tech. J.* **1964**, *43*, 1783–1809. [CrossRef]